Spectral band selection and classifier design for a multispectral imaging laser radar

Russell C. Hardie
University of Dayton
Department of Electrical and Computer Engineering
300 College Park Avenue
Dayton, Ohio 45469-0226
E-mail: rhardie@engr.udayton.edu

Mohan Vaidyanathan
Paul F. McManamon, MEMBER SPIE
U.S. Air Force Wright Laboratory
Electro-Optics Sensor Technology Branch (WL/AAJT)
Building 622, 3109 P Street
Wright-Patterson Air Force Base, Ohio 45433-7700

Abstract. A statistical spectral band selection procedure and classifiers for an active multispectral laser radar (LADAR) sensor are described. The sensor will operate in the 1 to 5 μm wavelength region. The algorithms proposed are tested using library reflectance spectra for some representative background materials. The material classes considered include both natural (vegetation and soil) and man-made (camouflage cloth and tar-asphalt). The analysis includes noise statistics due to Gaussian receiver noise and target induced speckle variations in the LADAR return signal intensity. The results of this analysis are then directly applied to an artificially generated spatial template of a scene consisting of these four material classes. The performance of four different classifier algorithms, which include a minimum distance classifier, a log-domain minimum distance classifier, a Bayes speckle-only classifier, and a Bayes speckle-Gaussian classifier, are evaluated. We show that the Bayesian classifier designed for speckle and Gaussian noise statistics outperforms the other classifiers. Our results also indicate that even when exact knowledge of the observation model is available, the classifier performance for speckled images can be poor unless the number of integrated speckle cells is large. [S0091-3286(98)00403-6]

Subject terms: active; multispectral; imaging laser radar; spectral band selection.

Paper ART-114 received May 29, 1997; revised manuscript received Aug. 19, 1997; accepted for publication Aug. 21, 1997.

1 Introduction

This paper describes the design and utility of an active multispectral laser radar (LADAR) sensor operating in the 1 to 5 μm wavelength region to image and identify ground targets. This sensor will especially be useful in high clutter situations where the target is partially concealed. The sensor will operate from an airborne platform capable of imaging ground targets at a range of up to 20 km. The sensor will exploit the unique reflectance spectrums of various materials for target discrimination. This reduces the sensor's reliance on classic geometric target detection/recognition techniques, which require high spatial resolution in high clutter situations. A number of challenges exist in the design and utilization of such a sensor, some of which are addressed in this paper.

While much work has been done in the area of passive multispectral target detection and identification,[1–7] the active LADAR system has many unique characteristics. An excellent overview of the current state-of-the-art LADAR technology, system design, and hardware is given by Osche and Young.[8] A description of the proposed active multispectral sensor, including phenomenology and system performance, is given by the authors elsewhere.[9]

The LADAR system observation model is not significantly a function of object emissivity or temperature as it is in passive IR systems.[4,5] This may be the single greatest advantage of such an active system. Thus it is possible to more directly interrogate an object's reflectivity in day or night in a way that is invariant to ambient illumination conditions. However, the LADAR system is subject to different types of noise sources partly due to the use of highly coherent illumination sources. These noise sources include optical receiver and electronic amplification noise sources, speckle effects, and atmospheric turbulence induced scintillation. The relative contribution of the individual noise sources is highly dependent on the sensor design, system parameters, target surface, and atmospheric conditions. In this paper, we analyze the effects of two predominant LADAR noise sources: signal independent Gaussian receiver noise and signal dependent target speckle fluctuations.[10]

This paper proposes a methodology for optimally selecting which spectral bands or wavelengths to use for the sensor. The band selection is based on an observation model, which includes material reflectance spectra, atmospheric transmission spectra and system parameters. In particular, a class separability metric is formulated and optimal wavelengths are selected using a forward sequential feature subset procedure.[11] A spectral Bayes classifier is defined that includes a model for target speckle[10] and Gaussian noise.

The organization of this paper is as follows. In Section 2, a direct-detection multispectral LADAR imaging sensor is described. Section 3 develops a statistical observation model, with Gaussian receiver noise and target speckle effects, for this sensor. Optimum spectral band selection for classifiers is addressed in Section 4. In Section 5, a Bayes classifier is defined based on our statistical model. Finally, simulation results and conclusions are presented in Sections 6 and 7, respectively.

 0091-3286/98/$10.00

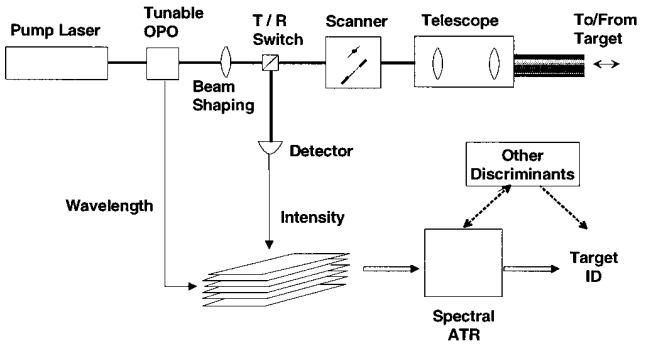

Fig. 1 Experimental layout of a direct-detection multispectral LADAR imaging system.

2 Sensor Description

The multispectral LADAR sensor will combine the principles of a conventional LADAR and a passive multispectral or hyperspectral remote sensor. Conventional LADARs and some passive imaging sensors use the geometrical shape of the target for recognition and identification. In contrast, the active multispectral LADAR will utilize the spectral characteristics of the target for identification purposes. The active multispectral sensor may be particularly advantageous in situations where the target is partially or mostly concealed. In such situations, the spatial shape correlation may have limitations or require higher sensor resolution. Furthermore, the active LADAR sensor may offer improved system sensitivity (i.e., signal to noise ratio or SNR) and it is less sensitive to diurnal and ambient effects.

The source wavelength, target reflectivity, and propagation losses are of primary importance in the design of this system.[9] The source wavelengths must be selected so that the LADAR will have minimal attenuation due to atmospheric molecules and aerosols, and battlefield induced obscurants. For common military smoke and dust aerosols, 3 to 5 μm wavelength region has smaller attenuation compared to shorter wavelengths. For source wavelengths less than 1 μm, atmospheric attenuation can be very strong compared to the mid-IR, particularly when the visibility is low. The 10 μm band could have some utility, but most materials have low reflectivity in this region and low-cost tunable compact laser sources are not readily available. For the subbands in the 1.3 to 5 μm wavelength region, most materials have relatively strong and characteristic features that could be utilized for effective spectral discrimination. Another advantage to the mid-IR region is its insensitivity to absolute humidity, as compared to the far-IR region. Furthermore, this wavelength subband is generally considered eye-safe and compact diode-pumped-laser sources that can be frequency shifted to produce highly efficient tunable radiation in this wavelength region are commercially available. As such, we investigate the 1 to 5 μm waveband as the operating regime for this sensor.

The principle of operation of this sensor is similar to that of a conventional laser-based sensor system, but with the added wavelength tuning capability using a tunable optical parametric oscillator (OPO) as the light source. The proposed LADAR layout is shown in Fig. 1. A short pulse (3 ns pulsewidth) 1 μm solid state Nd:YAG laser optically pumps an OPO source to produce tunable radiation in the 1.3 to 5 μm wavelength region. The OPO source is based on a new class of nonlinear optical material called periodically poled lithium niobate[9] (PPLN). Multispectral discrimination is achieved by tuning the OPO transmitter to the desired wavelengths. The LADAR receiver is a direct energy detection system designed to have very high sensitivity and a broad spectral response over the entire transmitter wavelength tuning range. The initial design of the LADAR system is a monostatic scanned imaging format using a tightly collimated beam illuminating the target. Two-dimensional multispectral image data sets (i.e., a spectral stack of 2-D scanned intensity images) are acquired by raster scanning a scene at a set of laser transmitter wavelength. The target's spectral information contained in each image pixel is extracted and fed to a spectral classifier algorithm. Classification is done on a pixel-by-pixel basis using the spectral classifier algorithm. Spatial and other discriminants may also be added to increase the robustness of classification.

3 Statistical Observation Model

The signal used for target detection and identification will be a measurement of optical return power at a set of N different wavelengths. Thus, it is important to begin our analysis by understanding the relationship between object reflectivity $\rho(\lambda)$ and the optical return power $\Phi_r(\lambda)$. The following section addresses this relationship.

3.1 *Optical Return Power*

The optical return power[12,13] for the LADAR system is given by

$$\Phi_r(\lambda)=\Phi_t(\lambda)\frac{A_{\text{targ}}}{r^2\Omega_{\text{trans}}}\frac{A_{\text{rec}}}{r^2\Omega_{\text{scatt}}}\eta_{\text{atm}}(\lambda)\varepsilon_{\text{sys}}(\lambda)\rho(\lambda). \quad (1)$$

The transmitted optical power is specified by $\Phi_t(\lambda)$, the area of the target is given by A_{targ}, and A_{rec} is the area of the receiver. The distance or range to the target is given by r. The parameters Ω_{trans} and Ω_{scatt} are the transmitted solid angle beamwidth and target scattering solid angle, respectively.[12] Note that diffuse targets are approximately Lambertian and scatter into 2π sr. However, in practice, the effective scattering solid angle Ω_{scatt} is generally taken to be π to account for the non-ideal fall off of intensity as the target angle moves away from normal.[12] The term $\eta_{\text{atm}}(\lambda)$ represents the round-trip atmospheric transmission function, and $\varepsilon_{\text{sys}}(\lambda)$ is the overall system optical efficiency.

Note that the range squared multiplied by the transmitted solid angle is the area of the beam at the target yielding

$$A_{\text{beam}}=r^2\Omega_{\text{trans}}. \quad (2)$$

Also, the receiver solid angle can be written as[12]

$$\Omega_{\text{rec}}=\frac{A_{\text{rec}}}{r^2}=\frac{\pi D^2}{4r^2}, \quad (3)$$

where D is the diameter of the receiver aperture. Substituting Eqs. (2) and (3) into Eq. (1) and manipulating terms yields

$$\Phi_r(\lambda)=\Phi_t(\lambda)\frac{A_{\text{targ}}}{A_{\text{beam}}}\frac{\Omega_{\text{rec}}}{\Omega_{\text{scatt}}}\eta_{\text{atm}}(\lambda)\varepsilon_{\text{sys}}(\lambda)\rho(\lambda). \quad (4)$$

For a fully resolved target, where the area of the target being illuminated is equal to that of the illumination beam (i.e., no illumination outside of the target), $A_{\text{targ}}=A_{\text{beam}}$. Using this and Eq. (3) and substituting $\Omega_{\text{scatt}}=\pi$, the optical return power can be expressed as

$$\Phi_r(\lambda)=\frac{D^2}{4r^2}\Phi_t(\lambda)\,\eta_{\text{atm}}(\lambda)\varepsilon_{\text{sys}}(\lambda)\rho(\lambda). \quad (5)$$

Consider evaluating Eq. (5) at N unique wavelengths $\lambda_1,\lambda_2,\ldots,\lambda_N$ yielding

$$\mathbf{z}=[z_1,z_2,\ldots,z_N]^T=[\Phi_r(\lambda_1),\Phi_r(\lambda_2),\ldots,\Phi_r(\lambda_N)]^T. \quad (6)$$

We shall assume that our active multispectral imaging system is calibrated to provide noisy measurements of $\mathbf{z}$ over a discrete spatial grid (via a scanning process). Let the noisy measurement vector at one particular spatial location be defined as $\mathbf{x}=[x_1,x_2,\ldots,x_N]^T$. It is from these measurements that we wish to perform target detection and identification.

3.2 *Noise Sources*

Now we discuss the LADAR noise sources. Ideally, optical receiver performance is limited by the photon or shot noise. In this case, the signal follows Poisson statistics. However, a practical direct-detection LADAR receiver is often limited by signal independent additive Gaussian noise.[14] This noise results from thermal or Johnson noise, dark current noise, or electronic amplifier noise.[12–14] In addition, the LADAR system may be subject to signal fluctuations due to target speckle and atmospheric turbulence. Signal variations due to target speckle results from the illumination of optically rough surfaces using highly coherent light sources.[10] LADAR signals propagating through turbulent atmospheric layers cause scintillation or intensity fluctuations in both transmit and receive propagation directions. Currently, to the best of our knowledge, there is no single unified theory or experimental data present in the literature characterizing the statistical behavior of all the just described noise sources combined. However, in many cases only one or two of the noise source is considered to be dominant. In the following analysis we consider two different cases: (1) signal independent Gaussian noise and (2) Gaussian noise with signal dependent target speckle effects. The following analysis considers the ideal case of a purely Lambertian or diffuse target surface and assumes that the signal develops from the illumination of the target with a single LADAR pulse from a single frequency (longitudinal mode) light source.

3.2.1 *Additive Gaussian noise*

It may be a sufficiently accurate approximation in some cases to model the overall noise as additive Gaussian noise.[14,15] In this case, a single spatial observation will be modeled as

$$\mathbf{x}=\mathbf{z}+\mathbf{n}, \quad (7)$$

where $\mathbf{n}=[\eta_1,\eta_2,\ldots,\eta_N]^T$ contains Gaussian noise samples. For independent noise the noise covariance is of the form

$$\mathbf{C}_n=\begin{bmatrix}\sigma_{\eta_1}^2 & 0 & 0 & \cdots & 0\\ 0 & \sigma_{\eta_2}^2 & 0 & \cdots & 0\\ 0 & 0 & \sigma_{\eta_3}^2 & \cdots & 0\\ \vdots & \vdots & \vdots & & \vdots\\ 0 & 0 & 0 & \cdots & \sigma_{\eta_N}^2\end{bmatrix}. \quad (8)$$

Note that $\sigma_{\eta_i}^2$ is the noise variance for spectral band i. The multivariate probability density function (pdf) of $\mathbf{x}$ is given by

$$P_{\mathbf{x}}(\mathbf{x})=\frac{1}{(2\pi)^{N/2}|\mathbf{C}_n|^{1/2}}\exp\left[-\frac{1}{2}(\mathbf{x}-\mathbf{z})^T\mathbf{C}_n^{-1}(\mathbf{x}-\mathbf{z})\right]. \quad (9)$$

In cases where the speckle phenomena can not be neglected, a different statistical development must be pursued. This is addressed in the following subsection.

3.2.2 *Gaussian noise with speckle effects*

It has been shown that the pdf of integrated speckle patterns can be well approximated by a gamma density.[10,14] Under certain conditions, the speckle can be modeled as multiplicative noise.[10,16,15] When both speckle and additive Gaussian noise are considered, the statistical modeling becomes more cumbersome; this case was analyzed by Mecherle.[14]

Let us begin by specifying the gamma pdf for integrated speckle patterns.[10] Let s_i represent the speckle signal for spectral band i. The pdf for this is given by

$$P_{s_i}(s_i)=\begin{cases}\dfrac{1}{\Gamma(M)}(M/z_i)^M s_i^{M-1}\exp\left(-\dfrac{Ms_i}{z_i}\right) & \text{for } s_i\geq 0\\ 0 & \text{for } s_i<0\end{cases}, \quad (10)$$

where M is the total number of speckle correlation cells that are observed during a measurement[14,10] (spatial, temporal, and also spectral, if a polychromatic source is used) and $\Gamma(\cdot)$ is the Gamma function. The observed value with additive Gaussian noise is given by

$$x_i=s_i+\eta_i, \quad (11)$$

for $i=1,2,\ldots,N$. Assuming the zero-mean Gaussian noise and the speckle patterns are independent, the pdf of x_i is obtained by convolving the pdfs of s_i and η_i. In particular,

$$P_{x_i}(x_i)=P_{s_i}(x_i)*P_{\eta_i}(x_i)=\int_{s=0}^{\infty}P_{s_i}(s)P_{\eta_i}(x_i-s)\,ds. \quad (12)$$

Plugging in the gamma and Gaussian pdfs yields

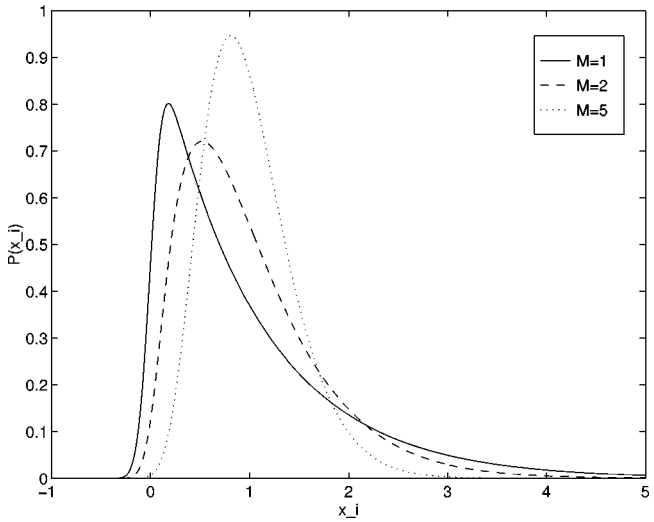

Fig. 2 The pdf $P_{x_1}(x_1)$ with speckle effects and Gaussian noise where $m_{s_1}=1$ and $\sigma^2_{\eta_1}=0.01$.

$$P_{x_i}(x_i)=\frac{(M/z_i)^M}{\Gamma(M)\sqrt{2\pi}\sigma_{\eta_i}}\int_{s=0}^{\infty} s^{M-1} \times\exp\left[-\frac{Ms}{z_i}-\frac{(x_i-s)^2}{2\sigma^2_{\eta_i}}\right]ds. \tag{13}$$

Unfortunately, there is no simple closed form expression for this integral. However, Mecherle[14] showed that the result can be written in terms of a parabolic cylinder function, and therefore, refers to $P_{x_i}(x_i)$ as a parabolic cylinder density. Using numerical integration, this pdf is evaluated and plotted in Fig. 2 for several values of M. Note, as M increases, the pdf appears more and more Gaussian in nature (although not signal independent). Increasing $\sigma^2_{\eta_i}$ has the same effect. This supports the notion that for larger values of M or $\sigma^2_{\eta_i}$, a Gaussian statistical model for the observed signal may be appropriate. Mercherle[14] also showed that the mean of x_i is given by $E(x_i)=z_i$. The variance is given by

$$\sigma^2_{x_i}=E(x_i^2)-E(x_i)^2=\frac{z_i^2}{M}+\sigma^2_{\eta_i}. \tag{14}$$

For our multispectral system, we assume that the speckle patterns and additive Gaussian noise are independent in each spectral band (as the bands may be acquired at different time intervals and at different wavelengths). This enables us to define the multivariate pdf as simply the product of the marginal densities,

$$P_{\mathbf{x}}(\mathbf{x})=\prod_{i=1}^{N} P_{x_i}(x_i). \tag{15}$$

The covariance of $\mathbf{x}$ in this case is given by

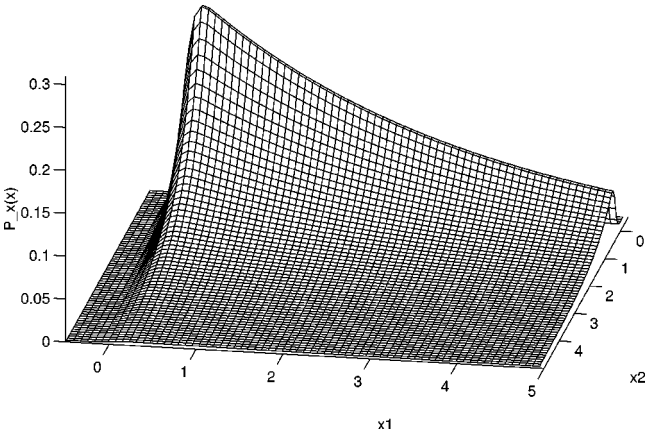

Fig. 3 The pdf $P_{\mathbf{x}}(\mathbf{x})$ with speckle effects and Gaussian noise where $\mathbf{z}=[3,1]^T$, $\sigma^2_{\eta_1}=\sigma^2_{\eta_2}=0.01$ and $M=1$.

$$\mathbf{C}_x=\begin{bmatrix}\sigma^2_{x_1} & 0 & 0 & \cdots & 0\\ 0 & \sigma^2_{x_2} & 0 & \cdots & 0\\ 0 & 0 & \sigma^2_{x_3} & \cdots & 0\\ \vdots & \vdots & \vdots & & \vdots\\ 0 & 0 & 0 & \cdots & \sigma^2_{x_N}\end{bmatrix}, \tag{16}$$

where $\sigma^2_{x_i}$ is given by Eq. (14). Figure 3 shows a 2-D pdf in the case where $\mathbf{z}=[3,1]^T$, $\sigma^2_{\eta_1}=\sigma^2_{\eta_2}=0.01$ and $M=1$. Note the increased kurtosis in the x_1 dimension, since the mean and variance are larger in that dimension.

The primary objective of the active multispectral sensor is to perform target identification for each noisy spatial observation $\mathbf{x}$. We would also like to specify which spectral bands will provide the best performance for a particular set of materials of interest. Thus, with the observation model and observed signal pdfs defined, we now address the problem of spectral band selection.

4 Optimum Band Selection

An ideal band selection criteria is minimum probability of error for the selected classifier and statistical observation model. However, computing the probability of error, even for a two-class Gaussian problem, is very cumbersome. In fact, for a two-class Gaussian problem, error bounds such as the Bhattacharyya bound[11] are generally used in lieu of a true probability of error. The Bhattacharyya bound metric has been used for band selection in passive systems.[6,7] No such simple bound exists for multiclass problems, where we wish to distinguish among several classes of materials. In this case, a practical approach may be to use a class separability metric based on the within-class and between-class scatter matrices.[11] This is described next.

4.1 *Separability Criteria*

To begin, assume we have L classes of materials to discriminate. Thus, a recognition algorithm must distinguish between L hypotheses denoted $H_1, H_2, \ldots, H_L$. Hypothesis H_k is that the observation vector $\mathbf{x}$ belongs to class k, for

$k=1,2,\ldots,L$. We assume that the only difference in the observations from different classes results from the different object reflectivity spectrums. Furthermore, variability of reflectivity spectrums for materials within a specified material class is not considered here. It is assumed that the exact target reflectivity is known. Let the noise and speckle free optical return power $\mathbf{z}$ specifically from class k be defined as

$$\mathbf{z}_k=[z_{k,1},z_{k,2},\ldots,z_{k,N}]^T. \tag{17}$$

Also, let the within-class scatter matrix be defined as

$$\mathbf{S}_w=\sum_{k=1}^{L} P_k E\{(\mathbf{x}-\mathbf{z}_k)(\mathbf{x}-\mathbf{z}_k)^T|H_k\}=\sum_{k=1}^{L} P_k \mathbf{C}_{x_k}, \tag{18}$$

where P_k is the *a priori* probability of observing class k, and $\mathbf{C}_{x_k}$ is the covariance for observations from class k. Note that $\mathbf{z}_k$ is the observation mean for class k and $\mathbf{C}_{x_k}$ can be obtained from Eq. (16) or Eq. (8), depending on the noise model. The between-class scatter matrix measures the scatter of mean vectors as

$$\mathbf{S}_b=\sum_{k=1}^{L} P_k(\mathbf{z}_k-\overline{\mathbf{z}})(\mathbf{z}_k-\overline{\mathbf{z}})^T, \tag{19}$$

where $\overline{\mathbf{z}}$ is the mean vector of the mixture distribution given by

$$\overline{\mathbf{z}}=\sum_{k=1}^{L} P_k\mathbf{z}_k. \tag{20}$$

These scatter matrices can be computed from the statistical models in Section 3. It is also possible to estimate these from empirical training data. In this case, the sample mean and covariance can be used.[11]

We have chosen as a measure of class separability the following metric[11]

$$J=\mathrm{tr}(\mathbf{S}_w^{-1}\mathbf{S}_b), \tag{21}$$

where $\mathrm{tr}(\cdot)$ represents the trace operation. A large J implies large between class separation relative to the within class scatter. Such a data distribution will clearly lead to improved classification. Although the J metric does not relate directly to the probability of error, we believe that it does offer a practical and effective quantitative measure of class separability.

4.2 *Forward Sequential Band Selection*

We define the optimal spectral bands to be those that lead to observations that maximize the value of J in Eq. (21). Assume there are N candidate bands of which K are to be selected for use. The number of candidate bands will generally be determined by what empirical observations are available or by the spectral resolution with which the observation model can be practically evaluated. The number of possible K band combinations, which could be used for our sensor, is given by

Table 1 Forward sequential spectral band selection procedure using the J separability criteria in (21).

Step 1:	Select the band which has the highest individual J value of the N candidate bands.
Step 2:	Pair each of the remaining $N-1$ candidate bands with the one selected in step 1. Select the band that yields the highest J in the 2-D band space.
Step 3:	Pair the remaining $N-2$ bands with the two selected and choose the band that yields the highest J in 3-D band space.
Step 4:	Continue in this fashion until K bands have been selected.

$$\frac{N!}{K!(N-K)!}. \tag{22}$$

An exhaustive search over all band combinations using the J separability metric would yield the optimal K band combination. However, this is impractical for anything but small values of K. A more practical, but suboptimal, method is outlined in Table 1. This is a forward sequential feature selection algorithm.[11] The number of J values to be computed with this method is given by

$$K\left(N-\frac{1}{2}K+\frac{1}{2}\right). \tag{23}$$

The forward sequential band selection method in Table 1 can be used with any class separability metric. This forward sequential method does a good job in most cases. However, if the globally optimal band set does not contain the first selected band, the solution may be far from optimal. One modification, which can make the algorithm more robust, is to do an exhaustive search to find the optimal P band set, where $1\leqslant P\leqslant K$. The forward sequential method can then be used to find the remaining $K-P$ bands. This compromise approach requires

$$\frac{N!}{P!(N-P)!}+(K-P)\left[N-\frac{1}{2}(K-P)+\frac{1}{2}\right] \tag{24}$$

J value computations.

5 Bayes Classifier Design

Here we describe two different Bayes classifiers[11] for the observation models defined in Section 3. The Bayes decision rule chooses the hypothesis $H_{k_{\max}}$ that maximizes the following *a posteriori* probability

$$k_{\max}=\arg\max_k \frac{P_{\mathbf{x}}(\mathbf{x}|H_k)P_k}{P_{\mathbf{x}}(\mathbf{x})}. \tag{25}$$

Note the denominator in Eq. (25) is not a function of k. Thus, the decision rule can be written as

$$k_{\max} = \arg \max_k P_{\mathbf{x}}(\mathbf{x}|H_k) P_k, \tag{26}$$

where $\mathbf{x}$ is the observation under test.

5.1 *Bayes Classifier for Gaussian Noise*

In the case of signal independent Gaussian noise only, the likelihood function based on Eq. (9) is given by,

$$P_{\mathbf{x}}(\mathbf{x}|H_k) = \frac{1}{(2\pi)^{N/2}|\mathbf{C}_n|^{1/2}} \times \exp\left[-\frac{1}{2}(\mathbf{x}-\mathbf{z}_k)^T \mathbf{C}_n^{-1}(\mathbf{x}-\mathbf{z}_k) \right], \tag{27}$$

where $\mathbf{C}_n$ is given by Eq. (8). In this case, it is more convenient (and equivalent) to minimize the minus natural log of the functional in Eq. (26). This yields

$$k_{\max} = \arg \min_k \{ -\ln[P_{\mathbf{x}}(\mathbf{x}|H_k)] - \ln(P_k) \}. \tag{28}$$

Substituting the Gaussian likelihood function into Eq. (28) and eliminating constant terms, the decision rule is given by

$$k_{\max} = \arg \min_k [(\mathbf{x}-\mathbf{z}_k)^T \mathbf{C}_n^{-1}(\mathbf{x}-\mathbf{z}_k) - \ln(P_k)]. \tag{29}$$

If the *a priori* probabilities are equal and the noise variance is equal in all bands and for all classes, this reduces to a simple minimum distance classifier.

5.2 *Bayes Classifier for Speckle and Gaussian Noise*

In the case of speckle only, the Bayes classifier can be defined based on Eq. (10) as

$$k_{\max} = \arg \max_k P_{\mathbf{x}}(\mathbf{x}|H_k) P_k = \arg \max_k \left[P_k \prod_{i=1}^{N} \left(\frac{M}{z_{k,i}} \right)^M x_i^{M-1} \exp\left(-\frac{M x_i}{z_{k,i}} \right) \right], \tag{30}$$

where constant terms are eliminated. Using the density function in Eqs. (13) and (15), the Bayes classifier for the case of speckle and Gaussian noise is given by

$$k_{\max} = \arg \max_k \left\{ P_k \prod_{i=1}^{N} \frac{1}{\sigma_{\eta_i}} \left(\frac{M}{z_{k,i}} \right)^M \int_{s=0}^{\infty} s^{M-1} \times \exp\left[-\frac{Ms}{z_{k,i}} - \frac{(x_i - s)^2}{2\sigma_{\eta_i}^2} \right] ds \right\}. \tag{31}$$

Again, all the constant terms have been eliminated in Eq. (31).

6 Simulation Results

To demonstrate the band selection procedure described in Section 4 and the classifiers described in Section 5, we present some simulation results here. For this analysis, we have selected four classes of materials with the spectral reflectances shown in Fig. 4. These data include 210 spectral samples over the wavelength range of 1 to 5 μm. Atmospheric corrections are then applied to these spectra. The atmospheric attenuation results from a variety of factors including molecular absorption, scattering, fog, precipitation, dust, etc. Several useful atmospheric models such as moderate resolution atmospheric transmission (MODTRAN) and high resolution atmospheric transmission (HITRAN) have been developed at Air Force Phillips Laboratories, Hanscom Air Force Base. Here, MODTRAN is used and provides a wavenumber spectral resolution of $2\,\mathrm{cm}^{-1}$ for molecular and aerosol constituents. The MODTRAN atmospheric transmission data were resampled to match the wavelengths of the library reflectance spectra shown in Fig. 4. The computed one-way atmospheric transmission spectra in the 1 to 5 μm wavelength range are shown in Fig. 5 for two different meteorological visibility

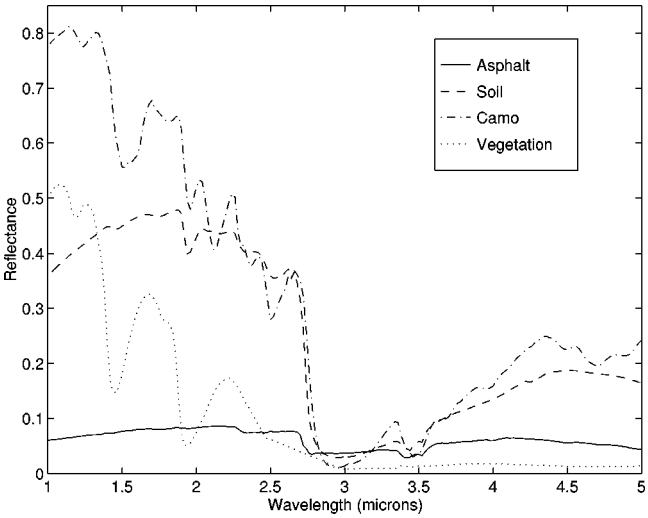

Fig. 4 Reflectance spectra in the 1 to 5 μm wavelength range for the four material classes studied in Section 6.

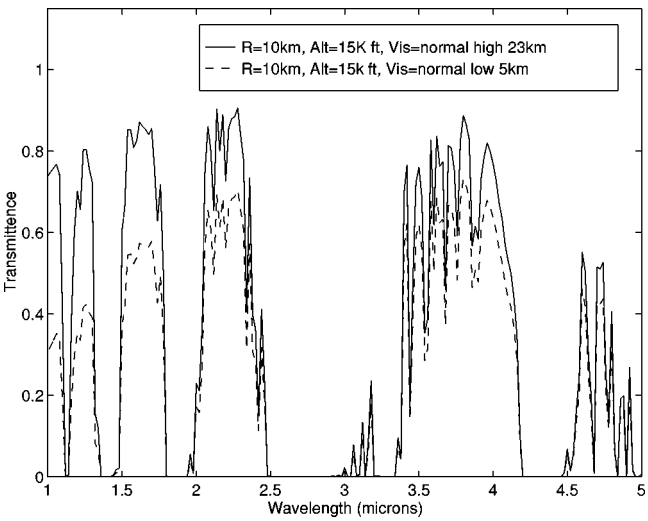

Fig. 5 One-way atmospheric transmission spectra computed using MODTRAN. The simulations correspond to a slant range of 10 km and an altitude of 15,000 ft and two different visibility conditions.

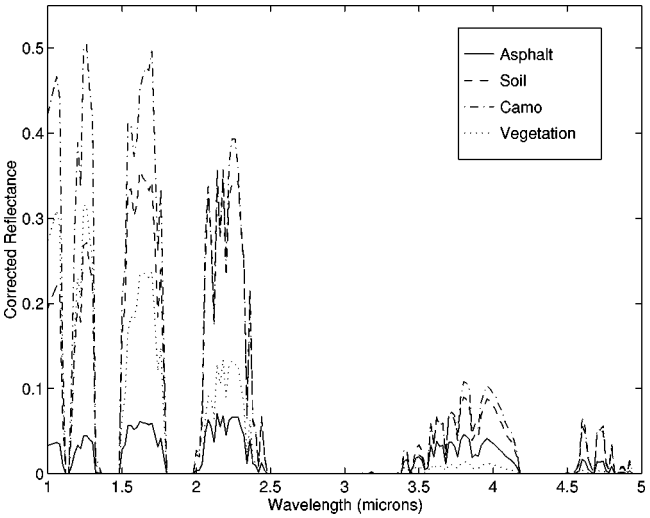

Fig. 6 Two-way atmospherically corrected class reflectance spectra. The atmosphere is modeled using MODTRAN for a slant range of 10 km, altitude of 15,000 ft, and a visibility of 23 km.

conditions. The class spectra with two-way atmospheric correction (range 10 km, altitude of 15,000 ft and visibility of 23 km) are shown in Fig. 6.

To complete the observation model described in Section 3, we assume that the system is calibrated such that

$$\frac{D^2}{4r^2}\Phi_t(\lambda)\varepsilon_{\text{sys}}(\lambda)=1. \tag{32}$$

Thus, the optical return power effectively reduces to the atmospherically corrected spectral reflectances. This assumption is based partly on the fact that for objects occupying the same range-bin, $D^2/4r^2$ is a constant. Also, it may be possible to control the wavelength dependent transmitted power $\Phi_t(\lambda)$ to compensate for variations in the system efficiency $\varepsilon_{\text{sys}}(\lambda)$.

Unless specifically stated otherwise, we use $M=10$ and $\sigma^2_{\eta_i}=0.0015$ for $i=1,2,\ldots,N$ for our simulation results. Considering only the Gaussian noise and a target with reflectivity of 0.25 at 1.00 μm, the SNR is 20 dB. First, let us consider the results for spectral band selection, and next, the results for the classifiers are presented.

6.1 *Band Selection*

An exhaustive search over the two-band space from 1 to 5 μm yields the separability surface shown in Fig. 7. The height of this surface at each point represents the separability J for that particular spectral wavelength pair. The largest separability occurs at 1.00 and 2.08 μm, although several other band pairs in the 1.00 to 2.5 μm range also yield good separability. Note that the lower wavelength of 1.00 μm is not readily accessible with current state-of-the-art sensors. However, a nearby wavelength of 1.064 μm matches with an emission line of the Nd:YAG laser. Our analysis indicates that the J value for 1.064 μm is still large (see Fig. 7).

A scatter plot showing the simulated noisy observations from each class in the optimal three-band space (1.00, 2.08, and 2.06 μm) is provided in Fig. 8 for $M=10$ and $\sigma^2_{\eta_i}=0.0015$. Note that there appears to be good class separability based on subjective evaluation of the data distribution. Also note that since the mean for the soil and cloth classes are relatively high, so are their variances (due to speckle). Thus, these classes have a higher within-class scatter compared to the asphalt and vegetation classes.

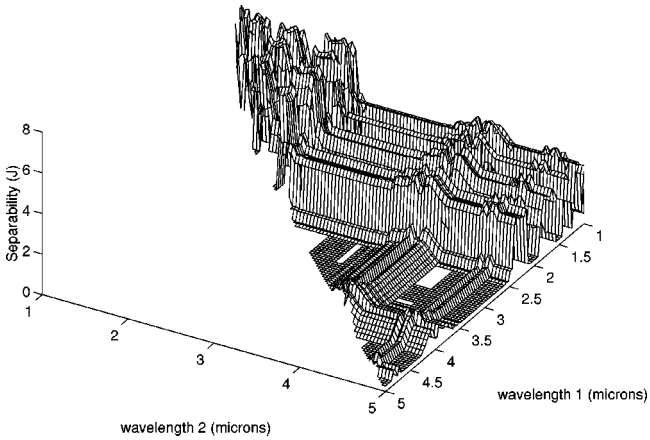

Fig. 7 Class separability surface showing the separability J for each spectral wavelength pair from 1 to 5 μm for $M=10$ and $\sigma^2_{\eta_i}=0.0015$.

To explore the effect of noise level and speckle on class separability, several simulations were performed. In particular, Fig. 9(a) shows the peak class separability in the case of Gaussian noise only at various levels. At each noise level the separability using the optimum three bands is shown. Clearly, separability is reduced as the noise level increases. Note that when $\sigma^2_{\eta_i}=0.0015$, the separability is approximately 45 (with no speckle effects). Figure 9(b) shows the peak class separability for the case of Gaussian noise ($\sigma^2_{\eta_i}=0.0015$) and speckle with different values of M. Note the poor separability for low values of M. When $M=\infty$, we get the Gaussian noise only case ($J=45$).

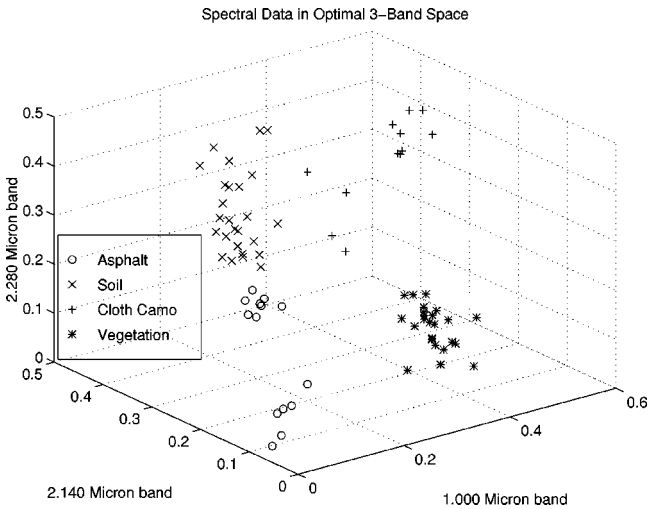

Fig. 8 Simulated observed data from each class in the optimal three-band space.

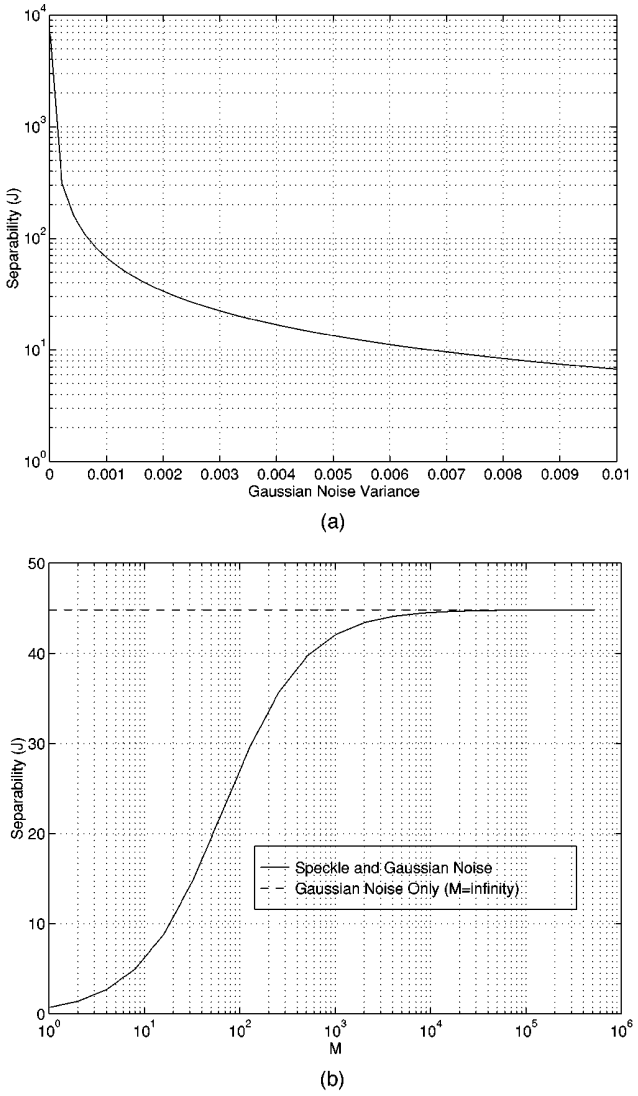

Fig. 9 Peak class separability using three spectral bands as a function of (a) Gaussian noise variance σ_η^2 with no speckle effects and (b) the speckle parameter M with Gaussian noise where $\sigma_{\eta_i}^2 = 0.0015$.

Note that for different materials, different noise levels, or different atmospheric conditions, the peak separability tends to vary in magnitude and often results from different spectral bands. Thus, the results presented in this section apply only for the specific parameters described here. However, we believe that the band selection procedure demonstrated here can be readily extended to a variety of other scenarios.

6.2 *Classifier Performance*

In this section, the performance of four classifiers is tested using simulated observations. Of primary interest is to evaluate the effect of speckle and Gaussian noise on classifier performance.

Consider the four classes of materials, shown in Fig. 4, arranged according to the spatial template shown in Fig. 10(a). Each class is coded with a different gray level. Using the atmospherically corrected reflectance spectra, shown in Fig. 6, three spectral band images were simulated. These are shown in Figs. 10(b) to 10(d) at the optimal wavelengths calculated in the previous section. Again, $M = 10$ and $\sigma_{\eta_i}^2 = 0.0015$.

Using the images in Fig. 10, the following four classifiers were tested: the minimum-distance classifier given by Eq. (29), the log-domain minimum-distance classifier, the Bayes speckle classifier in Eq. (30), and the Bayes speckle-Gaussian classifier in Eq. (31). The log-domain minimum-distance classifier is obtained by simply applying the minimum-distance classifier in Eq. (29) to the data in the log domain. This is done because the multiplicative component of the speckle becomes additive in the log domain.[15] Based on the central limit theorem, this additive component can be approximated as Gaussian.[15,17] This idea is the basis for homomorphic filtering of speckle images in image restoration applications.[15] In general, this approach will not perform as well as the optimum Bayes speckle-Gaussian classifier, but it does offer a relatively simple way to improve the performance of the minimum-distance classifier in some cases.

The class maps for the minimum-distance classifier in Eq. (29) and the optimal Bayes speckle-Gaussian classifier from Eq. (31) are compared in Fig. 11. Equal class *a priori* probabilities were used for all classifiers. The speckle-Gaussian classifier clearly outperforms the minimum distance classifier, which does not take into account the statistics of the speckle.

The probability of error is estimated by comparing the results for each classifier with the known template in Fig. 10(a). These results are shown in Fig. 12 for various values of M. The speckle only classifier yields the highest error. Thus, even though the level of Gaussian noise is relatively small, it clearly cannot be neglected in classifier design. The minimum-distance classifier, which neglects the speckle effects also produces a relatively high probability of error. The log-domain minimum-distance classifier does show improvement over the regular minimum-distance classifier.

The effect of using different numbers of bands on the probability of error is illustrated in Fig. 13. The optimal bands are used for each simulation. Performance clearly improves when more bands are used. Also note that the Bayes speckle-Gaussian classifier yields better results compared to the other three classifiers.

7 Conclusions

We formulated a methodology for band selection for a multispectral LADAR sensor and tested the method using library reflectance spectra of some representative background materials. The material classes considered include both natural (vegetation and soil) and man-made (camouflage cloth and tar-asphalt). The analysis included consideration of Gaussian receiver noise and target induced speckle variations in the LADAR return signal intensity. The results of this analysis were then directly applied to an artificially generated spatial template of a scene consisting of these four material classes. The performance of four different classifier algorithms, which included a minimum distance classifier, a log-domain minimum distance classifier, Bayes speckle-only classifier, and Bayes speckle-Gaussian

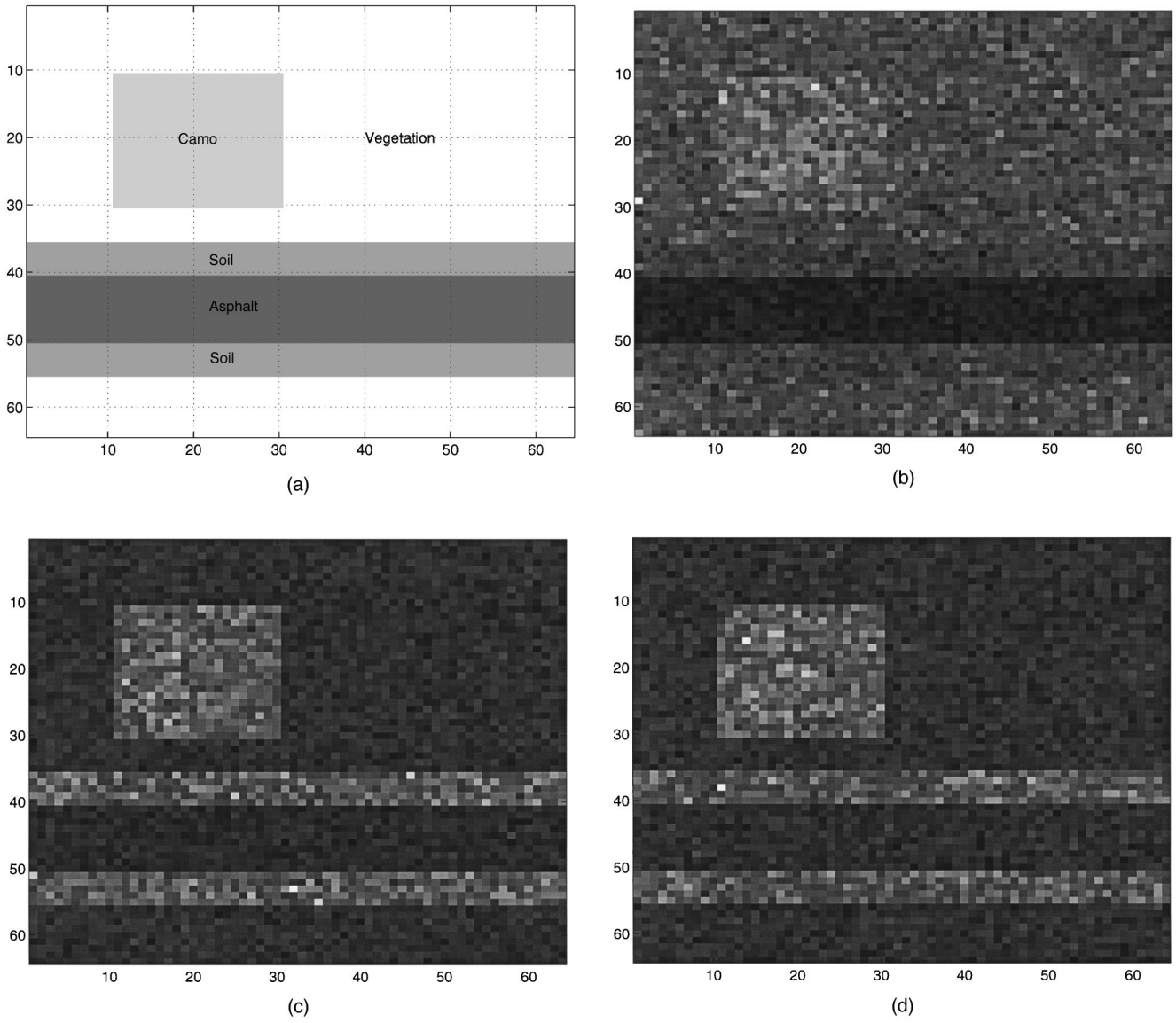

Fig. 10 (a) Four class spatial template used for classifier analysis. Each class is represented by a different gray level. The simulated speckled images ($M=10$ and $\sigma^2_{\eta_i}=0.0015$) are at (b) $\lambda=1.00$ μm, (c) $\lambda=2.06$ μm, and (d) $\lambda=2.08$ μm.

classifier, were evaluated. The Bayesian classifier designed for speckle and Gaussian noise statistics outperformed the other classifiers.

Our results also indicate that even when exact knowledge of the observation model is available, the classifier performance for speckled images can be poor unless the number of speckle cells or averaging parameter M is large. Thus, the speckle effect must be considered for the performance evaluation of the sensor and methods to mitigate its influence may have to be adopted. For typical direct detection LADAR systems, temporal (pulse or frame) averaging and spatial (aperture) averaging were implemented so that the speckle effect was reduced. In addition, the illumination of the target with sufficiently broad spectral bandwidth or multiple frequency (longitudinal mode) light source, such as the OPO system (with spectral bandwidth of the order of $10\ \mathrm{cm}^{-1}$) described earlier, could also suppress the speckle effect further in these direct detection systems. As such, we predict that it is feasible to obtain somewhat reduced speckle images by a proper design of the LADAR system for target identification.

It is important to recognize the fact that our simulation results represent the most ideal case. More specifically, it is assumed that we have exact knowledge of the reflectivity spectrum of the target materials, the atmospheric conditions, and the noise statistics. In practice, the exact knowledge of these parameters may not be known. Further, the target is assumed to be diffuse (i.e., ideally Lambertian). Many man-made target materials exhibit diffuse plus some specular characteristics. Thus, the simulations presented here represent a best case analysis. Notwithstanding this,

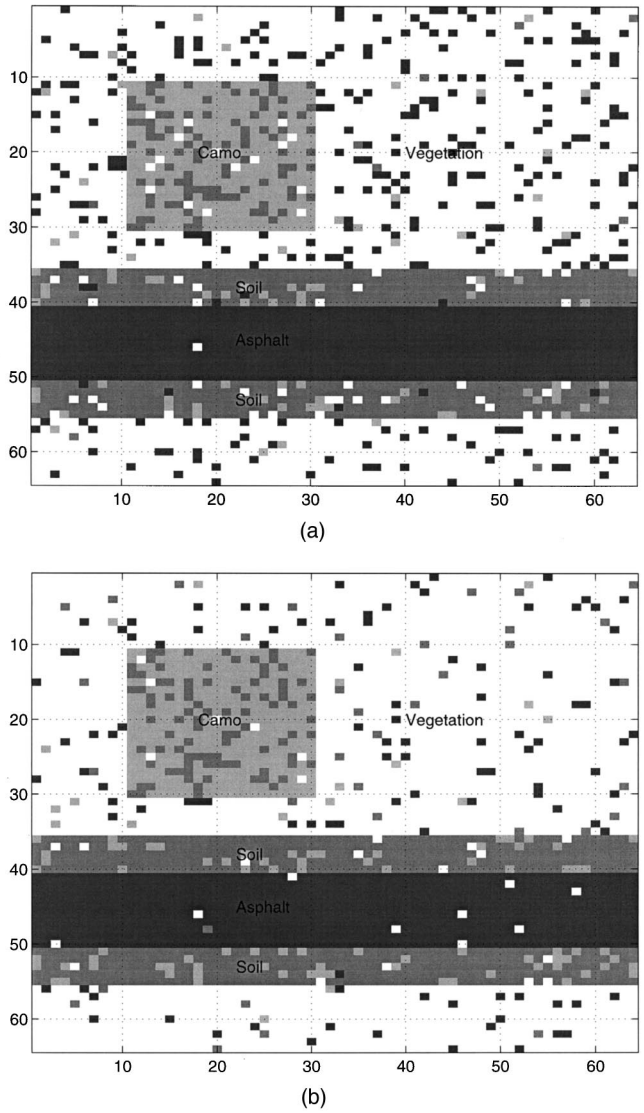

Fig. 11 Class maps for classifiers operating on the three simulated image bands in Fig. 10: (a) minimum distance classifier output and (b) Bayesian speckle-Gaussian classifier output.

the simulations do highlight the key factors in classifier design for an active multispectral system.

In realistic applications, varying levels of knowledge about current atmospheric transmission and the reflectivity spectrum of the desired objects will be available. For example, these functions may only be known to within a scaling constant. In this case, a generalized classifier that estimates the unknown scaling constant while simultaneously doing the classification can be employed.[5] If less information is known, it may only be possible to perform outlier detection (rather than classification).[5,6]

Another, perhaps important, aspect of the LADAR system design is the number of wavebands to use for the sensor. As our initial analysis shows, classifier performance improves with the addition of wavebands in the multispectral data set. The number of wavebands required for good performance may also depend on the number of classes present in the scene. Furthermore, the number of wavebands that can be used with the sensor is limited by the practical issues of tuning the transmitter wavelength as well as the cost and speed of the sensor system.

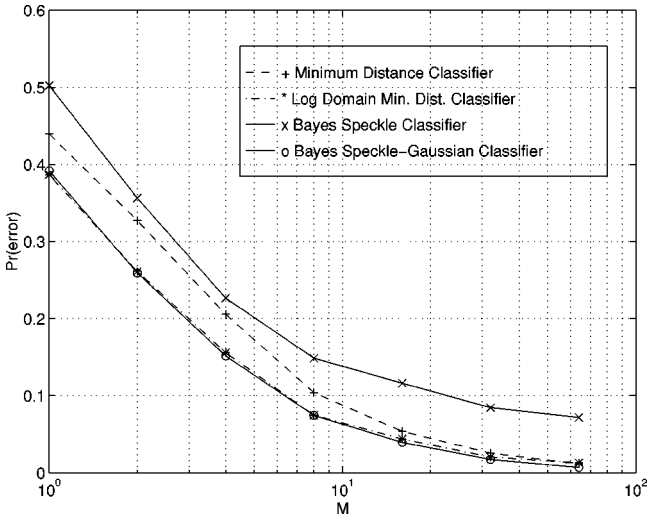

Fig. 12 Probability of error for several classifiers using the three-band simulated data shown in Fig. 10.

In the future, we intend to extend this work by incorporating additional material classes in our analysis. The goal will be to find some set of wave bands that will yield the best performance for a wide range of relevant scenarios. The influence of atmospheric turbulence induced scintillation statistics on the classifier performance will also be studied. We also plan to examine the case where only partial information about the class spectra is known. Using the methodology described here, the effect of using different spectral bandwidths, system parameters and high resolution atmospheric spectra can be studied. Ground truth field measurements, when available, will also be incorporated in these future investigations.

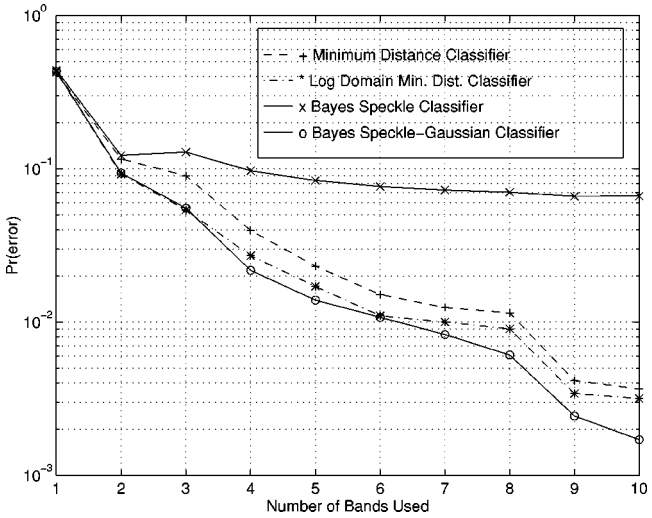

Fig. 13 Probability of error for several classifiers using various numbers of simulated image bands. The optimal bands for speckle and Gaussian noise are used in each case ($M=10$ and $\sigma^2_{\eta_i}=0.0015$).

Acknowledgments

Dr. Mohan Vaidyanathan acknowledges the support provided by the National Research Council Air Force Office of Scientific Research associateship programs. Dr. Russell Hardie has been supported under Air Force contract no. F33601-95-DJ010. The authors would like to thank Dr. Tim Grayson for his helpful advice and support in the early stages of this project. Thanks also to Dr. Ray O. Johnson and Dr. Mike Eismann who provided great insight into band selection for passive multispectral systems. Thanks also to Drs. Ed Watson and Mohammad Karim for supporting this project.

References

1. J. A. Richards, *Remote Sensing Digital Image Analysis*, Springer-Verlag, Berlin (1986).
2. X. Jia and J. Richards, ''Efficient maximum likelihood classification for imaging spectrometer data sets,'' *IEEE Trans. Geosci. Remote Sens.* **32**, pp. 274–281 (Mar. 1994).
3. B. Kim and D. Landgrebe, ''Hierarchical classifier design in high-dimensional, numerous class cases,'' *IEEE Trans. Geosci. Remote Sens.* **29**, pp. 518–528 (July 1991).
4. I. S. R. X. Yu and A. D. Stocker, ''Comparative performance analysis of adaptive multispectral detectors,'' *IEEE Trans. Signal Process.* **41**, pp. 2639–2656 (Aug. 1993).
5. X. Yu, L. E. Hoff, I. S. Reed, and A. M. C. L. B. Stotts, ''Automatic target detection and recognition in multiband imagery: a unified maximum likelihood detection and estimation approach,'' *IEEE Trans. Image Process.* **6**, pp. 143–156 (Jan. 1997).
6. R. C. Hardie, ''Adaptive quadratic classifiers for multispectral target detection,'' U.S. Air Force Summer Faculty Program 1994 Final Report, Vol. 5A (1994).
7. A. Kanodia, R. C. Hardie, and R. O. Johnson, ''Band selection and performance analysis for multispectral target detection using truthed bomem spectrometer data,'' in *Proc. IEEE National Aerospace Electronics Conf. (NAECON)*, Dayton, OH (May 1996).
8. G. R. Osche and D. S. Young, ''Imaging laser radar in the near and far infrared,'' *Proc. IEEE* **84**, pp. 103–125 (Feb. 1996).
9. M. Vaidyanathan, T. Grayson, R. Hardie, L. Myers, and P. McManamon, ''Multispectral laser radar development and target characterization,'' *Proc. SPIE* **3065**, 255–266 (Apr. 1997).
10. J. C. Dainty, *Laser Speckle and Related Phenomena*, Springer-Verlag (1984).
11. K. Fukunaga, *Introduction to Statistical Pattern Recognition*, Academic Press, San Diego (1990).
12. C. G. Bachman, *Laser Radar Systems and Techniques*, Artech House, (1979).
13. S. A. McDonald, ''Comparison of apd and fiber pre-amplified pin detectors for direct detection ladar systems,'' Masters Thesis, University of Dayton (Dec. 1996).
14. G. S. Mecherle, ''Signal speckle effects on optical detection with additive gaussian noise,'' *J. Opt. Soc. Am.* **1**, pp. 68–72 (Jan. 1984).
15. A. K. Jain, *Fundamentals of Digital Image Processing*, Prentice Hall, Englewood Cliffs, NJ (1989).
16. M. Tur, K. C. Chin, and J. W. Goodman, ''When is speckle noise multiplicative,'' *Appl. Opt.* **21**, pp. 1157–1159 (Apr. 1982).
17. A. Papoulis, *Probability, Random Variables, and Stochastic Processes*, 2nd ed., McGraw-Hill, New York (1984).

Russell C. Hardie received a BS (Magna Cum Laude) from Loyola College, Baltimore, in 1988, an MS in electrical engineering from the University of Delaware in 1990, and a PhD in electrical engineering from the University of Delaware in 1990. Dr. Hardie is currently an assistant professor in the Department of Electrical and Computer Engineering at the University of Dayton. Prior to teaching at the University of Dayton, Dr. Hardie was a senior scientist with Earth Satellite Corporation (EarthSat) in Rockville, Maryland. His research interests include signal and image processing, IR and multispectral imaging systems, nonlinear filters, adaptive filter theory, pattern recognition and remote sensing.

Mohan Vaidyanathan received his MS and PhD degrees from Rensselaer Polytechnic Institute and University of South Florida, respectively. His primary research has been in the area of spectroscopy and laser remote sensing. Presently he is a National Research Council/Air Force Office of Scientific Research (AFOSR) associate at the Sensors Directorate, Air Force Research Laboratory, Wright-Patterson Air Force Base, Ohio. His current research includes development of lasers and optical parametric oscillator devices, laser radar sensors, and image processing for target recognition.

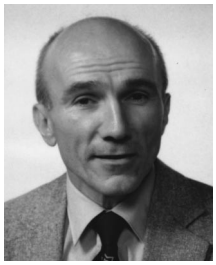

Paul F. McManamon received his PhD in physics from Ohio State University in 1977. He was with Wright Patterson Air Force Base from 1968 to 1979 when he joined Wright Laboratory, where his primary work has been in electro-optical sensors. Recently he has done more work with laser radar sensors than with passive IR sensors, but has research interests in both areas. He was acting as associate chief scientist for the Avionics Directorate of Wright Laboratory for over two and a half years. He is currently tech director for the Electro-Optics Division of the Sensors Directorate, Air Force Research Laboratory.